

Ferrimagnetic cluster formation due to oxygen vacancies in $\text{CaFe}_2\text{O}_{4-\delta}$

Rajasree Das,¹ Saikat Debnath,^{2,3} G. Narsinga Rao,^{1,4} Shobhana Narasimhan,² and F. C. Chou^{1,5,6,*}

¹Center for Condensed Matter Sciences, National Taiwan University, Taipei 10617, Taiwan

²Theoretical Sciences Unit and School of Advanced Materials, Jawaharlal Nehru Centre for Advanced Scientific Research, Jakkur, Bangalore 560064, India

³Department of Physics, M.V. College, Buxar, Bihar 802101, India

⁴Department of Physics, M.L.R Institute of Technology and Management, Hyderabad, Telangana, India

⁵National Synchrotron Radiation Research Center, Hsinchu 30076, Taiwan

⁶Taiwan Consortium of Emergent Crystalline Materials, National Science Council, Taipei 10622, Taiwan

 (Received 25 August 2016; revised manuscript received 7 September 2018; published 3 October 2018)

CaFe_2O_4 possesses an intriguing crystal structure characterized by the presence of FeO_6 octahedra that share both edges and corners, and featuring zigzag Fe chains that are assembled in a honeycomb tube network. The nominal CaFe_2O_4 has been identified to show a long-range antiferromagnetic spin ordering of Néel temperature $T_N \sim 184$ K. From dc and ac magnetic susceptibility measurements on both polycrystalline and single-crystal samples, a random distribution of ferrimagnetically ordered clusters of Fe spins is proposed to exist in the oxygen deficient $\text{CaFe}_2\text{O}_{4-\delta}$. The ferrimagnetic ordering is proposed, coming from the oxygen vacancy-induced Fe^{3+} to Fe^{2+} conversion for the antiferromagnetically coupled spins of Fe^{2+} ions in the low-spin state and the Fe^{3+} ions in the high-spin state, which leads to an incomplete cancellation of staggered magnetization below T_N . Current model reasonably explains the inconsistencies found in the literature regarding the persistent ferromagnetic component for CaFe_2O_4 , having a confirmed antiferromagnetic long-range spin ordering from neutron diffraction studies. We calculate the antiferromagnetic spin structure and the parameters of a Heisenberg Hamiltonian via spin-polarized density functional theory, obtaining results that are consistent, to a very high degree, with our experimental results for ac and dc magnetic susceptibility.

DOI: [10.1103/PhysRevB.98.144404](https://doi.org/10.1103/PhysRevB.98.144404)

I. INTRODUCTION

Calcium ferrite, CaFe_2O_4 , is a versatile material that has been investigated for its intriguing structural, electronic, magnetic, and chemical properties since its crystal structure was first reported [1]. Its wide variety of applications include use as a component in electronic devices [2], as a catalyst for several reactions [3,4], as a photocathode for the hydrogen evolution reaction in water splitting [5,6], as a ceramic pigment and coating [7], and as the electrodes of solid oxide fuel cells [8].

Unlike many ferrites, it does not crystallize in the spinel structure, nor does it crystallize in the perovskite structure, as many transition metal oxides do. Instead, it forms in an orthorhombic structure, which is notable for the presence of zigzag Fe chains running along the b direction, and the FeO_6 octahedra that share both edges and corners to form a three-dimensional honeycomb tube network (see Fig. 1). The Fe^{3+} ions are expected to have a spin moment $S = 5/2$ for the preferred half-filled $3d^5$ configuration, and the Fe-zigzag chains are arranged in a honeycomb pattern as hexagonal tunnels extending along the b direction, with a slightly flattened distortion along the c direction [9].

We note that such zigzag chains and the edge-/corner-shared octahedra are also found as motifs in the crystal structures of the isochemical compounds CaT_2O_4 , where T is a transition metal (T = Ti, V, Cr, Mn, or Co). These compounds

display a range of magnetic couplings and different types of magnetic ordering, which are found to be very sensitive to both the size of the transition metal ions and the magnitude of the spins [10–16].

Although the magnetic properties of CaFe_2O_4 have been previously studied by several groups, there does not appear to be a consensus in the literature about either the type of magnetic ordering or the magnetic transition temperatures. Some authors have postulated the coexistence of two types of spin structure [17,18], labeled *A* and *B*. Both structures feature antiferromagnetic (AF) ordering between the neighboring Fe-zigzag chains; however, the coupling within the chain is ferromagnetic (FM) in *A* but AF in *B*. It has also been suggested that the competition between these phases results in the formation of solitary magnons [18]. The *A* and *B* phases were reported as having Néel temperatures T_N of 170 K and 200 K, respectively [17,18]. These results differ from those of an earlier neutron diffraction study in which two magnetic transitions at 140 K and 285 K were identified [19]. However, it has also been suggested that the observed transition at 140 K could arise from the inclusion of an impurity phase of $\text{Ca}_2\text{Fe}_2\text{O}_5$ [20].

Recently, we have successfully grown high-quality single crystals of CaFe_2O_4 by using the optical floating zone method [21]. In this paper, we report ac and dc magnetic susceptibility measurements for these samples and the results of accompanying calculations using *ab initio* spin-polarized density functional theory. Our results indicate the presence of only one magnetic phase transition, with the low-temperature

*shobhana@jncasr.ac.in; fcchou@ntu.edu.tw

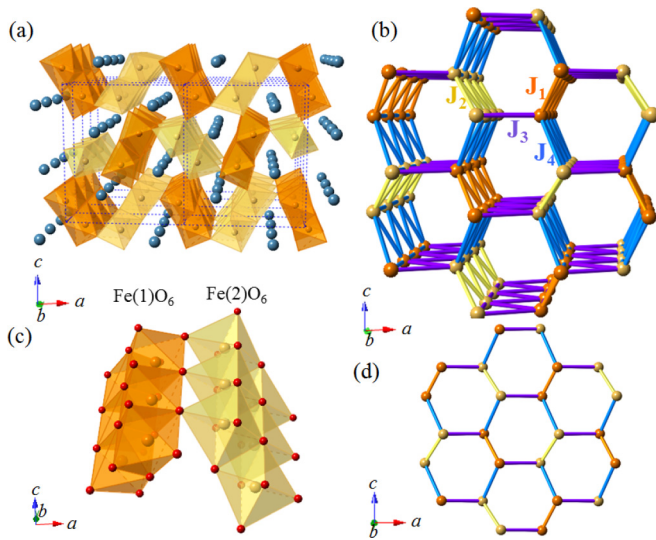


FIG. 1. Crystal structure of CaFe_2O_4 . (a) shows the edge- and corner-sharing FeO_6 octahedra, with Ca atoms (colored blue online) occupying the interstitial sites. The two sets of octahedra (colored orange and yellow online) are centered around Fe(1) and Fe(2) atoms, respectively. (b) shows Fe-zigzag chains running along the b axis to form hexagonal tunnels arranged in a distorted honeycomb lattice. (c) shows a zoomed-in view of the $\text{Fe}(1)\text{O}_6$ and $\text{Fe}(2)\text{O}_6$ octahedra in chain along the b direction, with the oxygen atoms depicted as small spheres. (d) shows a projection of (b) onto the ac plane. The exchange couplings J_1 , J_2 , J_3 , and J_4 are labeled in (b). The complete bond lengths and bond angles are given in Table I.

phase having AF spin ordering with $T_N \sim 184$ K. Below this temperature, we observe peculiar thermal and magnetic hysteresis of a nontrivial FM moment; we believe that this is due to the inevitable presence of oxygen vacancies under the specified growth condition. When there is a missing O atom, the magnetic moment on the neighboring Fe atoms is significantly reduced, approaching a value more typical of Fe^{2+} . As a result, the net magnetic moment per unit cell becomes nonzero and spins order antiferromagnetically below T_N , which suggests that the magnetic ordering of the system might be canted AF or ferrimagnetic (FI) clusters, rather than strictly AF.

To verify this interpretation, we have also deliberately introduced a tunable proportion of oxygen vacancies to examine how the magnetic properties vary with the oxygen stoichiometry. Our interpretation of how the magnetic properties are affected upon the introduction of oxygen vacancies is also supported by our calculations. Although the question of oxygen nonstoichiometry in calcium ferrite has been studied before [22,23], these earlier studies were carried out in oxygen-rich conditions, and therefore considered the possibility of having an excess of oxygen atoms, rather than a deficiency. The impact of varying oxygen concentration on magnetic properties was also not explored systematically.

II. EXPERIMENTAL DETAILS

High-quality CaFe_2O_4 single crystals were grown using the traveling solvent floating zone technique in an O_2 atmosphere (~ 0.32 MPa). Details of the preparation conditions have

been reported by us previously [21]. The oxygen vacancy levels were tuned by annealing the as-grown single crystals in vacuum or in oxygen at high temperatures. Thermal analysis of the as-grown single crystals in Ar flow (NETZSCH TG-DTA system) indicated that a significant amount of oxygen vacancies could be generated by annealing above 700°C without decomposition. Samples with a relatively high proportion of vacancies were prepared through the postannealing of the as-grown samples, which were sealed in an evacuated quartz tube.

The chemical composition of the single crystals was analyzed using an electron probe microanalyzer (EPMA) with ten-point average per scan of error bar size ± 0.02 . The crystals were found to have a chemical composition of $\text{CaFe}_2\text{O}_{4-\delta}$, where δ was 0.06 for the as-grown crystal, and δ had values of 0.18 and 0.24 for crystals that were vacuum annealed at 750°C for ~ 10 h and ~ 20 h, respectively.

Room temperature synchrotron x-ray powder diffraction (SXRD) patterns were collected at the National Synchrotron Radiation Research Center in Taiwan, using a source with $E = 18$ keV and $\lambda = 0.6889$ Å. Rietveld refinement was performed using the GENERAL STRUCTURE ANALYSIS SYSTEM software package. Upon refining the structure, we find that the orthorhombic phase of CaFe_2O_4 belongs to the $Pnma$ space group, and has lattice constants that are consistent with those reported in the literature [21].

Both dc and ac magnetic susceptibilities were measured using a SQUID-VSM (Quantum Design, USA).

III. RESULTS AND DISCUSSION

A. Crystal structure

CaFe_2O_4 has been confirmed to crystallize in an orthorhombic structure with space group $Pnma$. The lattice constants of the as-grown sample are given in Table I, and are in excellent agreement with those reported in the literature [24].

The Fe atoms occupy two inequivalent sites within space group $Pnma$ and are labeled as Fe(1) and Fe(2) (see Fig. 1). There is a small difference in the average Fe-O bond length between $\text{Fe}(1)\text{O}_6$ and $\text{Fe}(2)\text{O}_6$ octahedra [see Fig. 1(c)]; we find these to be 2.030 Å and 2.043 Å, respectively. The resulting orthorhombic distortion corresponds to a mirror symmetry breaking along the c direction from the hexagonal symmetry of an ideal honeycomb lattice, as shown in the ac projection [see Fig. 1(d)]. Details of the experimentally determined structure are given in Table I.

B. Magnetic Susceptibility Experiments

1. Powder and crystal magnetization measurement

Magnetization measurements on powder samples were performed to eliminate the complication of orbital anisotropy in the Curie-Weiss law data analysis. The powder samples were prepared by crushing the as-grown single crystal samples [21]. The magnetization M and homogeneous magnetic susceptibility ($\chi = M/H$) as a function of temperature in various applied magnetic fields are shown in Fig. 2. According to the Curie-Weiss law, the temperature dependence of the magnetic susceptibility in the paramagnetic (PM) regime is

TABLE I. Experimental results based on SXRD data refinement for the crystal structure and theoretical results for the exchange couplings J_i . Here χ^2 , R_p , and R_{wp} are the profile fitting parameters representing goodness of fit, the profile, and the weighted profile, respectively. The superexchange paths $b1$ and $b2$ are parallel to the b axis and connect alternate atoms along the Fe(1) and Fe(2) zigzag chains, respectively. Exchange paths 1, 2, 3, and 4 connect adjacent Fe atoms along the zigzag chains (see Fig. 1), and five connects a Fe(1) atom with the next-nearest Fe(2) atom. The experimental values were previously published in Ref. [21].

Sample name	CaFe ₂ O ₄		$a = 9.2297(3) \text{ \AA}$	$\chi^2 = 3.609$
Crystal structure	Orthorhombic		$b = 3.0192(1) \text{ \AA}$	$R_p = 4.86\%$
Space group	$Pnma$		$c = 10.7028(4) \text{ \AA}$	$R_{wp} = 5.74\%$
Exchange path i	$l_i(\text{Fe-Fe})$ (\AA)	$\angle(\text{Fe-O-Fe})$ (deg)	$l(\text{Fe-O})$ (\AA)	Calculated J_i/k_B (K)
$b1$	3.019(3)	99.79(3);93.55(9)	2.072(7);1.974(4)	-1.08
$b2$	3.019(4)	95.16(5);93.92(7)	2.065(7);2.045(2)	-1.08
1	3.093(7)	99.44(6)	1.988(4); 2.065(2)	-4.19
2	3.102(1)	97.99(2)	2.072(3); 2.038(5)	-5.44
3	3.578(1)	121.81(2)	2.045(5); 2.050(3)	-14.69
4	3.649(2)	130.10(3)	2.051(6); 1.974(2)	-23.93
5	5.047(3)	$\angle(\text{Fe-O-O})$ 92.93(1);97.31(4)	Fe-O 2.065(3);2.050(1)	0.87

given by $\chi(T) = \chi_0 + C/(T - \Theta)$, where the temperature-independent χ_0 term includes the core diamagnetic (χ^{core}) and Van Vleck PM (χ^{VV}) contributions to the susceptibility (with the contribution from Pauli paramagnetism assumed

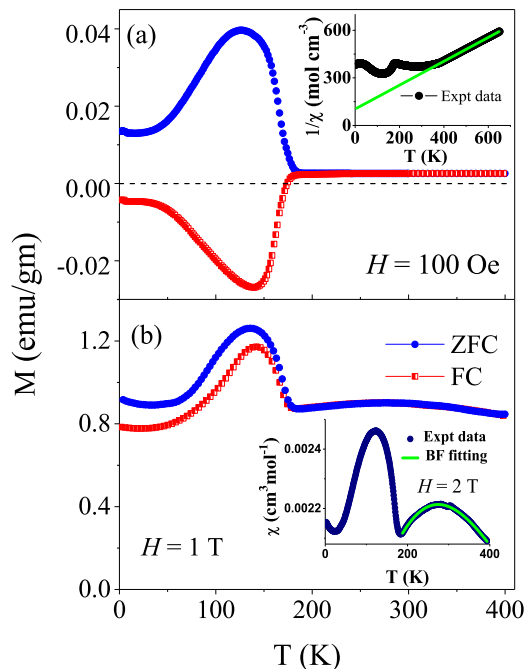


FIG. 2. Experimental results for the temperature dependence of the magnetization M and homogeneous magnetic susceptibility $\chi = M/H$. (a) Field-cooled (FC) and zero-field-cooled (ZFC) magnetization for the as-grown CaFe₂O_{4- δ} crushed crystals measured in an applied field of (a) 100 Oe (adapted from Ref. [21]) and (b) 1 T. The inset of (a) shows the $1/\chi$ vs temperature T relationship, and a negative intercept of $1/T$ in high temperatures above ~ 400 K suggests that the Weiss temperature $\Theta = -135$ K. The inset of (b) shows the fit obtained using the Bonner-Fisher model (see text) with a nearest-neighbor exchange constant $J = -27.2$ K.

to be equal to zero); i.e., $\chi_0 = \chi^{\text{core}} + \chi^{\text{VV}}$, C is the Curie constant, and Θ is the Weiss temperature. Upon fitting this formula to our data for the as-grown sample (with $\delta = 0.06$) in the high temperature range (300–650 K) above $2T_N$, as shown in the inset of Fig. 2(a), we obtain $\chi_0 = 6.77(2) \times 10^{-4} \text{ cm}^3/\text{mol}$, $C = 3.64(1) \text{ cm}^3 \text{ K}/\text{mol}$, and $\Theta = -135.02(5) \text{ K}$. The theoretical χ^{core} value estimated from $\chi^{\text{core}} = \chi_{\text{Ca}}^{\text{core}} + 2\chi_{\text{Fe}}^{\text{core}} + 4\chi_{\text{O}}^{\text{core}}$ suggests that χ^{VV} is of the order of $7.55 \times 10^{-4} \text{ cm}^3/\text{mol}$ [25,26]. An effective moment of $\mu_{\text{eff}} = 5.40(2) \mu_B$ per Fe ion (assuming that the gyromagnetic ratio $g = 2$) is derived from the Curie constant. In the absence of O vacancies, the Fe ions are expected to have a 3+ charge state and $S = 5/2$ for a half-filled $3d^5$ configuration in the high spin (HS) state, following Hund's rule. Because the theoretical value of μ_{eff} for Fe³⁺ ions in this HS state is $5.92 \mu_B$, the somewhat smaller value of μ_{eff} obtained in our experiments suggests that a small fraction of the spins must have $S < 5/2$. In addition, the negative Weiss temperature Θ signifies that the effective exchange coupling between spins is AF in the PM state.

Significant field dependence and thermal hysteresis between zero-field-cooled (ZFC) and field-cooled (FC) measurements are evident below ~ 184 K, as shown in Fig. 2. At low field, negative ZFC magnetization is observed below 184 K, which could be resulted from a FI ordering due to incomplete cancellation of AF ordered spins, or a canted AF ordering of high coercive field [23,27,28]. For a canted AF spin structure, the spin ordering is modified by an angle between the two equivalent magnetic sublattices and a FM component is acquired along the plane perpendicular to the AF ordering axis to show a sharp increase in χ near T_N [29,30]. On the other hand, for a ferrimagnet, the temperature dependence of the staggered magnetization for the AF ordered two sublattices may not be equivalent, which could lead to a peculiar temperature dependence of the net ZFC magnetization below T_N , as illustrated by the confirmed FI system Ni₃TeO₆ [28]. The T -dependence of magnetization for FI system which is shown by Sankar *et al.* as an example

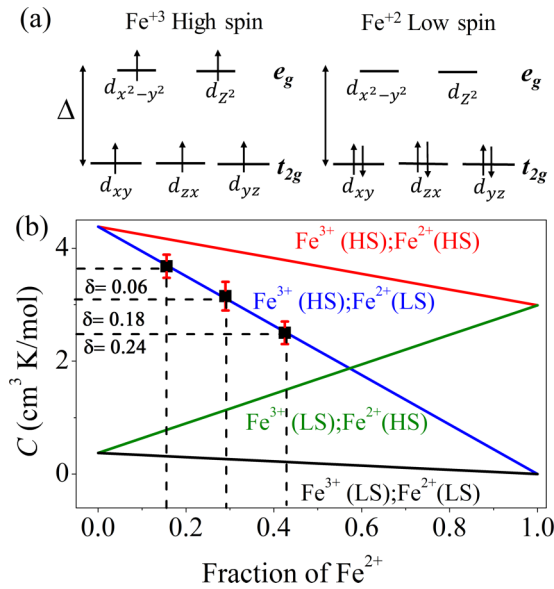


FIG. 3. High-spin (HS) and low-spin (LS) states. (a) The electronic configuration of the d electrons for Fe^{3+} (d^6) in HS and Fe^{2+} (d^6) in LS states in an octahedral crystal field. (b) Curie constant C as a function of Fe^{2+} concentration 2δ . The straight lines show the theoretically predicted values of C for four possible spin combinations of Fe^{3+} and Fe^{2+} ions in HS and LS states. The dashed lines correspond to three experimental values of C extracted from measurements on samples with oxygen vacancy concentration $\delta \sim 0.06, 0.18,$ and 0.24 .

for phenomenon of partial negative ZFC magnetization would not happen for a homogeneous canted AF system. Therefore, bearing the additional complication from the randomly distributed FI clusters of various sizes, the temperature dependence of the ZFC magnetization should not attribute to a canted AF system but can be explained more reasonably with the existence of FI ordered clusters.

By the requirement of charge neutrality, the presence of oxygen vacancies in $\text{CaFe}_2\text{O}_{4-\delta}$ is expected to introduce a proportional amount of Fe^{2+} following the relationship of $\text{CaFe}_{2-2\delta}\text{Fe}_{2\delta}^{2+}\text{O}_{4-\delta}$. For the Fe^{2+} ions with an electronic configuration of $3d^6$ in the octahedral crystal electric field (CEF) with e_g - t_{2g} splitting, a LS state of $S = 0$ is expected, as shown in Fig. 3(a). We therefore examine a few possible combinations of Fe charge and spin configurations and the resulting values of the Curie constant C as a function of the fraction of Fe^{2+} ions converted from Fe^{3+} due to the presence of oxygen vacancies with concentration δ , as shown in Fig. 3(b). There are four possible combinations of $\text{Fe}^{3+}/\text{Fe}^{2+}$: HS/HS, HS/LS, LS/HS, and LS/LS. Next, we plot our experimentally obtained C values for three samples with different oxygen vacancy concentrations of $\delta=0.06(2), 0.18(2),$ and $0.24(2)$. All three experimental points fall on the theoretical $C(\text{Fe}^{2+}$ fraction) line of $\text{Fe}^{3+}/\text{Fe}^{2+}$ in the HS/LS configuration. In particular, the deduced Fe^{2+} fractions projected from the three Curie constants using the proposed C - Fe^{2+} fraction (2δ) relationship [Fig. 3(b)] are $\sim 0.15, 0.29,$ and 0.42 , which are found to be in good agreement with those derived from the predicted values of 2δ obtained from the theoretical model using δ values extracted independently from the EPMA analysis.

These results strongly support the proposed model that oxygen vacancies introduce a proportional valence state change of Fe ions from Fe^{3+} in the HS = 5/2 state to Fe^{2+} in the LS = 0 state. As a result, the incomplete cancellation of the neighboring Fe spins in AF ordering could introduce the observed nonzero positive magnetization to the FC measurement sequence. The observed negative and irreversible ZFC magnetization at low field must result from the unsuccessful magnetization reversal in low field; i.e., the applied low field is below the required coercive field for the FM domain removal [31]. The combined evidence of the negative ZFC magnetization at low field and the negative Weiss temperature Θ in the PM state suggests that the magnetic phase transition for $\text{CaFe}_2\text{O}_{4-\delta}$ is possibly FI in nature. However, the negative ZFC magnetization should not be used as the sole supporting evidence for any long-range magnetic orderings. Negative ZFC magnetization does not occur persistently in the systems having FM, homogeneous FI, or canted AF orderings and may be treated as an artefact, especially when it is coming from the wrongly assigned zero field of unknown field trapped in the superconducting magnet. Since the possible existence of FI ordering in $\text{CaFe}_2\text{O}_{4-\delta}$ is proposed not to be homogeneous but contains randomly distributed FI clusters near the oxygen vacancy sites of various sizes, the antiphase domain boundaries would cause irreversibility on the measured ZFC magnetization.

Anisotropic magnetization measurements have been performed for the as-grown single crystal sample along the three major axes, as shown in Fig. 4. Based on the weak negative magnetization obtained from the ZFC measurement under low field along the b direction, the distribution of inhomogeneous FI clusters near oxygen vacancies is proposed to be dominant along the b -direction and to have a uniaxial spin anisotropy along that direction. Moreover, the magnetization along the a direction shows a relatively large FC moment, which could result from a weak field-induced spin canting of the antiferromagnetically ordered spins aligned along the b direction, or

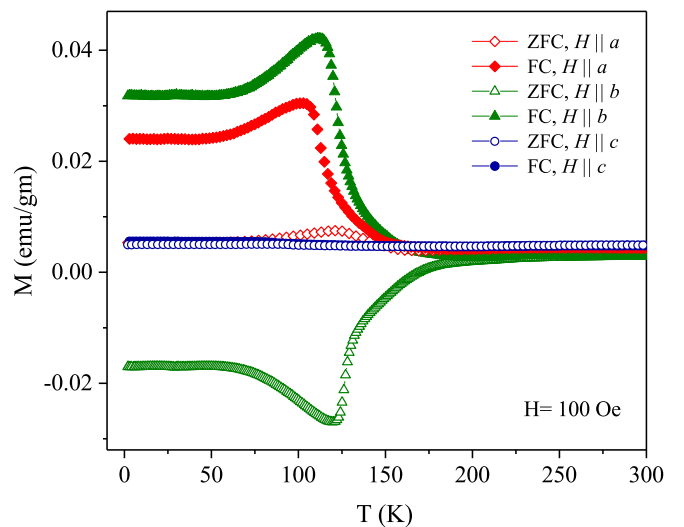


FIG. 4. Experimental values for the magnetization for the as-grown $\text{CaFe}_2\text{O}_{4-\delta}$ single crystal in a magnetic field of 100 Oe along three crystallographic axes, with ZFC (empty symbols) and FC (solid symbols) data. The negative M obtained in a ZFC measurement turns positive in FC measurement, suggesting a FI phase transition.

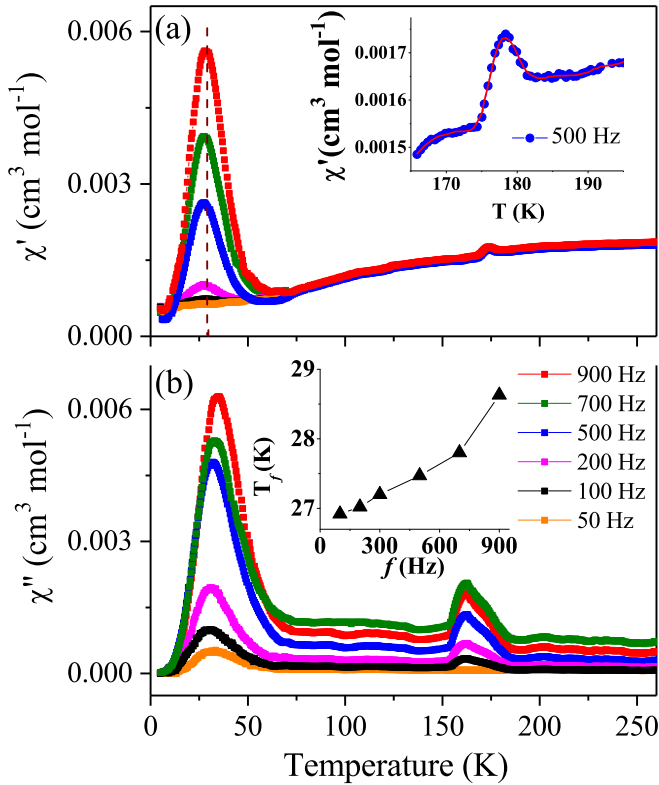


FIG. 5. Experimentally measured ac susceptibilities of $\text{CaFe}_2\text{O}_{3.94}$, $\chi'(T)$ in (a) and $\chi''(T)$ in (b), using the powder sample prepared from crushed as-grown single crystals in a zero dc applied field and ac field of 2 Oe at various ac frequencies. The inset of (a) shows a zoomed-in area near T_N , while the frequency dependence of the significant peak obtained at ~ 35 K is shown in the inset of (b).

from the spin system possessing an XY anisotropy. In fact, the existence of a layered structure is also supported by the presence of strong spin exchange interactions primarily within the ab plane of a corrugated armchair type, which will be presented further below in the theoretical section (Fig. 9).

2. ac susceptibility measurement

To verify if the system has FM, FI, or canted AF spin ordering at $T_N \sim 184$ K, the ac susceptibilities (real part χ' and imaginary part χ'') were measured using a powder sample prepared from the as-grown single crystals, as shown in Fig. 5. Because the ac field (2 Oe) in kHz range is too low for the FM moment or domain reorientation, the observed χ' displays a small peak near ~ 184 K with a concomitant onset of nonzero χ'' to indicate an exothermic phase transition, which suggests that the peak anomaly detected by the ac susceptibility signifies a magnetic phase transition that is AF in nature. Taken together, our measurements of dc and ac susceptibilities on $\text{CaFe}_2\text{O}_{4-\delta}$ appear to consistently support the scenario of an antiferromagnetically aligned FI spin ordering, not the canted AF.

Another notable feature in our results for χ' and χ'' is the presence of a broad frequency-dependent peak centered around ~ 35 K. Because the peak temperature shows a sensitive frequency dependence, similar to that found in spin glass

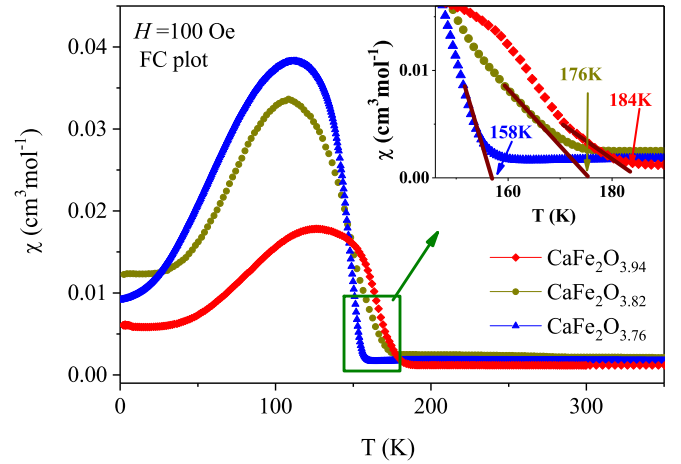


FIG. 6. Field-cooled (FC) data of dc homogeneous magnetic susceptibility ($\chi = M/H$) for as-grown and vacuum annealed CaFe_2O_4 crushed crystals in an applied magnetic field of 100 Oe. Inset shows that T_N is reduced from 184 K to 158 K with increasing oxygen vacancy level.

systems [32,33], we may infer that there are slow spin dynamics below the kilohertz range. The frequency dependence of the freezing temperature (T_f), as defined by the position of the peak in χ' , is displayed in the inset of Fig. 5(b). The positive frequency dependence of T_f suggests that there might be a spin-glass type frustration, which would then indicate the presence of a surprising re-entrant behavior below the long-range FI spin ordering. Although no low-temperature structural data are available, it is possible that the strain energy induced by the randomly distributed oxygen vacancies could become dominant at low temperatures, and frustration is likely to occur for spins near the vacancy sites of relatively stronger local distortion.

We find that the magnetic transition temperature (T_N) of $\text{CaFe}_2\text{O}_{4-\delta}$ depends strongly on the oxygen content. Based on the transition temperature defined by the onset of dc magnetization, T_N values for $\text{CaFe}_2\text{O}_{3.94}$, $\text{CaFe}_2\text{O}_{3.82}$, and $\text{CaFe}_2\text{O}_{3.76}$ are found to be ~ 184 K, 176 K, and 158 K, respectively, as shown in Fig. 6. T_N defined by the dc susceptibility data are consistent with those established from the χ'' in the ac measurement, as shown in Fig. 5. T_N decreases with increasing oxygen vacancy concentration, which agrees with the scenario that more vacancy defects are destructive to the magnetic ordering. Although the values of T_N for the nominal CaFe_2O_4 reported in the literature are inconsistent [17–19,23,34], we believe that the inconsistency is mainly due to the difference in oxygen content and/or the inclusion of impurity phase like $\text{Ca}_2\text{Fe}_2\text{O}_5$ [20]. In addition, T_N for a system with randomly distributed FI clusters should be defined as the onset of transition in dc magnetization curve or the corresponding onset of the χ'' peak obtained from the ac measurement [35].

C. Theoretical calculations

1. Calculation methods

Calculations for the electronic and magnetic structures of CaFe_2O_4 (both in the absence and presence of O vacancies)

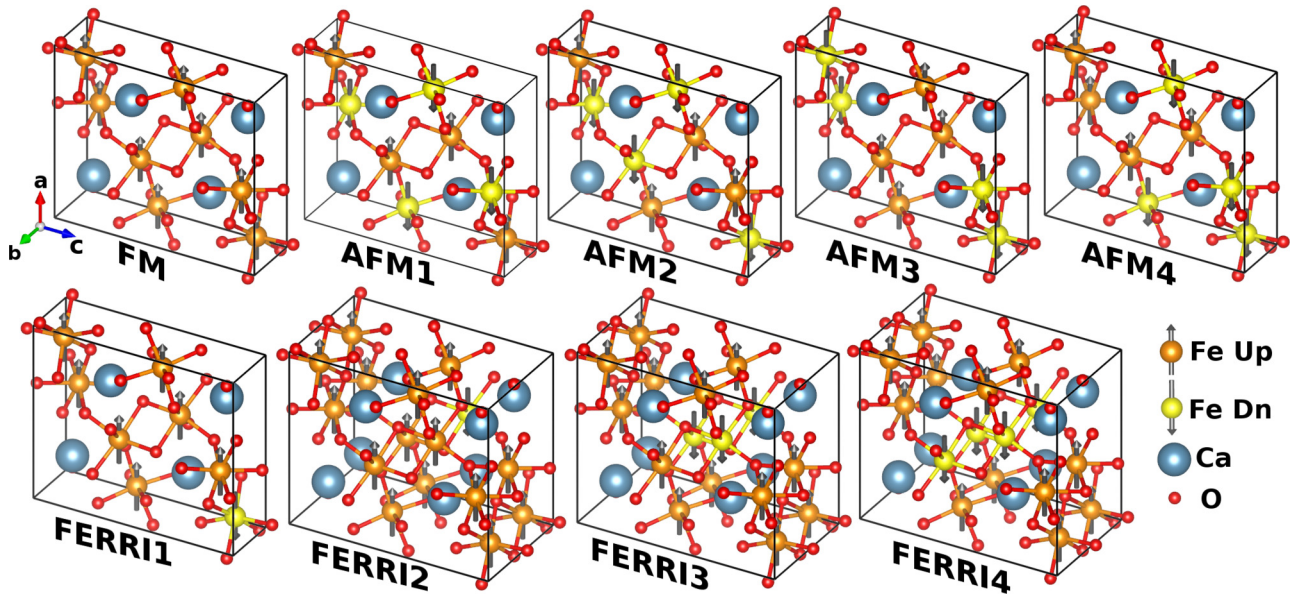


FIG. 7. The nine different magnetic configurations used to obtain the parameters of the Heisenberg model are shown. Up- and down-polarized magnetic Fe ions are shown as orange spheres with an up arrow, and yellow spheres with a down arrow, respectively. Ca and O atoms are denoted by large blue and small red spheres, respectively. Only nearest-neighbor Fe-O bonds are shown explicitly. Note that in the absence of spin-orbit interactions, the “up” and “down” directions are only notional. The magnetic unit cells for the FM, AFM1, AFM2, AFM3, AFM4, and FERRI1 configurations contain 28 atoms, whereas those for the FERRI2, FERRI3, and FERRI4 configurations contain 56 atoms.

were carried out within a plane wave pseudopotential implementation of density functional theory (DFT), using the Vienna *ab initio* simulation package (VASP) [36,37]. A plane-wave cutoff of 450 eV was employed. Projector-augmented wave [38,39] potentials were used, and the exchange correlation interactions were treated within the generalized gradient approximation (GGA) in the PBE form [40,41]. An additional on-site Coulomb interaction U of 4 eV was used on Fe- d states, as suggested by previous authors [42]. The Brillouin zone was sampled with a Monkhorst-Pack grid of $6 \times 18 \times 6$ k -points. Calculations were performed with the lattice constants fixed at the experimental values; however, all internal coordinates were optimized.

The effects of vacancy formation were investigated by introducing a single O vacancy at four inequivalent O sites of a $2 \times 2 \times 2$ supercell; this corresponds to considering $\text{CaFe}_2\text{O}_{4-\delta}$ with $\delta = 0.016$. We note that introducing the vacancy lowers the symmetry of the structure.

Several different starting magnetic configurations were considered; in all cases, the symmetry of the final magnetic configuration to which the system relaxed was found to be the same as that of the initial magnetic configuration.

2. Calculated spin structure

We first consider pristine CaFe_2O_4 in the absence of oxygen vacancies. To obtain the magnetic ground state and a database of energies from which exchange coupling constants can be extracted, we consider nine different magnetic configurations: one FM configuration, four different AF configurations (labeled as AFM1, AFM2, AFM3, and AFM4), and four different FI configurations (labeled as FERRI1, FERRI2, FERRI3, and FERRI4). The orientations of the magnetic

moments of the Fe atoms in these configurations are shown in Fig. 7; note that these directions are only notional, in the absence of spin-orbit interactions. The relative energies for these nine different collinear magnetic configurations are tabulated in Table II; note that all energies are referenced with respect to the FM configuration. The AFM1 configuration is the most stable; here, all Fe(1) ions have up-spins, whereas all Fe(2) ions have down-spins. AFM1 [see Fig. 8(a)] is the same as the A phase described by previous authors [17,18]. In all configurations, the magnitudes of the magnetic moments on individual Fe ions are found to be more or less the same; the

TABLE II. Relative energies E_{rel} for different magnetic configurations calculated using DFT (target values) and from the Heisenberg model (fitted values) with the seven parameters J_i described in the text. All energies are referenced to the FM configuration. The results from DFT calculations for the magnetic moment μ are also presented.

Config.	E_{rel} (meV/formula unit)		μ (μ_B /formula unit)
	DFT	Model	
FM	0	0	10.0
AFM1	-229.3	-230.6	0.0
AFM2	-120.3	-120.2	0.0
AFM3	-147.0	-146.9	0.0
AFM4	-130.3	-130.3	0.0
FERRI1	-63.5	-64.7	7.5
FERRI2	-33.1	-33.5	8.8
FERRI3	-92.3	-91.7	6.2
FERRI4	-118.0	-116.8	5.0

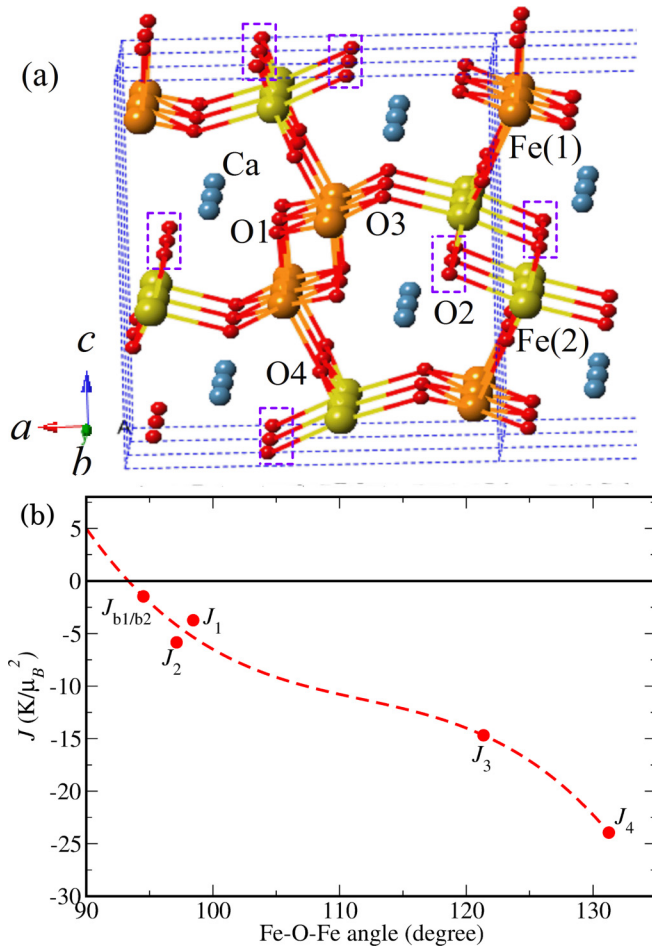


FIG. 8. (a) Unit cell for stoichiometric CaFe₂O₄ in the AFM1 magnetic structure. Up and down spin Fe atoms have been shown in orange spheres and yellow spheres, respectively. (b) Variation of superexchange interaction strength as a function of Fe-O-Fe angle. We find a monotonic change in superexchange interaction strength that seems to follow the Goodenough-Kanamori rules.

various configurations differ only in the relative orientations of the spins on individual Fe ions.

In a previous theoretical study [43], Obata *et al.* also found AFM1 (denoted as AFM_A in their paper) to be the lowest energy magnetic configuration. We note that for the most part, they compared total energies using results from GGA calculations, i.e., no U term was included. However, using a value of $U = 5.2$ eV, they found that the FM configuration was higher in energy than AFM1 by 205 meV per formula unit; this is close to our value of 230 meV per formula unit, obtained using $U = 4.0$ eV. Moreover, the corresponding results for the calculated magnetic moments of the Fe atoms in AFM1 are extremely close: they reported a value of $\pm 4.176 \mu_B$, while we obtain $\pm 4.2 \mu_B$.

Next, we use the results in Table II to determine the parameters of a Heisenberg model given by the Hamiltonian $H_{\text{mag}} = -\sum_{i,j} J_{ij} \mathbf{S}_i \cdot \mathbf{S}_j$, where J_{ij} is the coefficient of the magnetic exchange interaction between spins \mathbf{S}_i and \mathbf{S}_j at sites i and j , respectively. We consider seven magnetic exchange pathways between two Fe atoms, these correspond to the seven types of Fe-Fe pairs considered in Table I. Following the same labeling

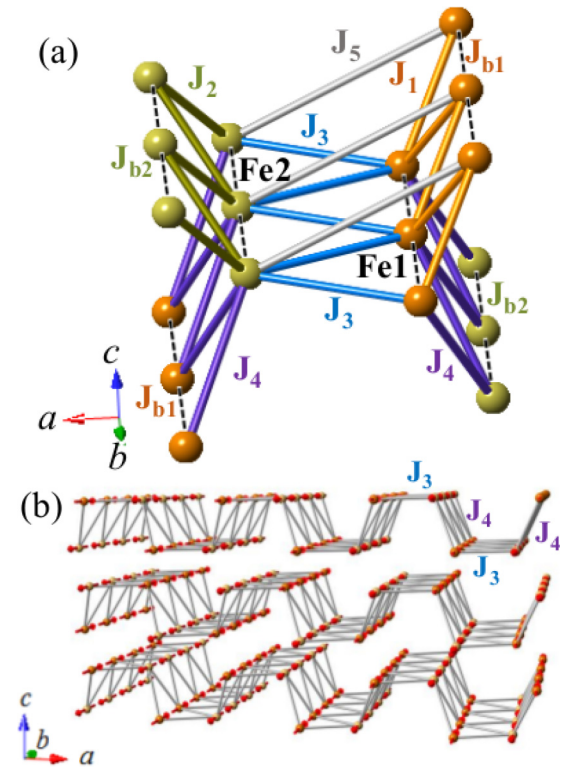


FIG. 9. (a) Schematic spin arrangement for the configuration AFM1 of CaFe₂O₄; note that the values of the exchange parameters J_i are tabulated in Table I. (b) A schematic drawing of the effective spin structure as an armchair-type plane in perspective view, where $J_3 = \alpha J_4$ with $\alpha = 0.61$.

convention as used in Table I and shown in Fig. 9(a), the seven distinct exchange constants are denoted as J_{b1} , J_{b2} , J_1 , J_2 , J_3 , J_4 , and J_5 . Upon fitting to the values from our *ab initio* calculations for the relative energies of the nine configurations considered, we obtain the values for these seven parameters expressed in temperature units as shown in Table I. Please note that the AFM1 (A phase) and previously mentioned B phase[18] are almost degenerate in energy, with the B phase being lower in energy by 7 meV/unit cell. While this is a somewhat surprising result, given that the A phase is expected to be the global minimum, we estimate this difference as being comparable to the limit of accuracy of our DFT calculations and has not been included in the model.

In contrast to the naive expectation that the values of the J_i s (where i labels the exchange pathways) should decrease with increasing inter-atomic distance l_i (Fe-Fe), we find that J actually increases with the relevant Fe-Fe distances for the first few terms (see Table I). For example, the magnitudes of J_{b1} and J_{b2} are smaller than those of J_1 , J_2 , J_3 , and J_4 , although the lengths of the exchange pathways are shorter for the former than the latter. We also note that all exchange constants are negative (indicating an AF interaction), except for the positive J_5 , thus indicating an FM interaction. J_5 corresponds to the shortest super-superoxchange pathway in the crystal, which is between Fe(1)-Fe(2) pairs separated by a distance of 5.03 Å, via an Fe(1)-O(1)-O(3)-Fe(2) network of super-superoxchange routes.

We find that the Fe-O-Fe bond angles play an important role in determining the exchange coupling strength. According to the Goodenough-Kanamori (GK) rules, a strong AF coupling is expected when two partially filled d orbitals overlap via completely filled p orbitals and the d - p - d angle is close to 180° , whereas a weak FM interaction prevails when the angle is close to 90° [44–46]. On plotting our results for J_i vs the relevant Fe-O-Fe angle θ [see Fig. 8(b)], the magnitude of J_i increases more or less smoothly with θ , which explains why most of the values of J_i obtained by us are negative, corresponding to AF interactions. On extrapolating the curve to 90° , we see that for this angle, J_i would be positive (FM coupling), as expected. This curve also explains why the magnitudes of the J_i values obtained by us increase as we advance from J_{b1} , J_{b2} to J_4 .

For the AFM1 spin structure, we can use our calculated values of J_i to estimate the Weiss temperature Θ within a mean field approximation. To accomplish this, we use the following equation [47] (see further details in the Supplemental Material [48]):

$$\Theta = \frac{S(S+1)}{3k_B} \sum_i z_i J_i, \quad (1)$$

where i runs over all symmetry-inequivalent types of exchange pathways retained, and z_i is the number of exchange pathways involving the corresponding exchange coupling constant J_i [see Fig. 9(a)]. This yields a calculated value $\Theta = -129$ K, which is indeed in good agreement with the value ($\Theta = -135$ K) obtained from fitting the magnetic susceptibility data in the high-temperature PM regime to the Curie-Weiss law.

3. Bonner-Fisher model fitting

The dominant exchange couplings are J_3 and J_4 ; these are at least one order of magnitude larger than the other couplings, as summarized in Table I for the J_i s defined in Fig. 9(a). Thus, it may be useful to look at the system as a series of armchair-type alternating chains built up by the dominant J_3 and J_4 , extending along the a direction, with weak interchain (J_{b1} , J_{b2}) and interplane (J_1 , J_2) couplings along the b and c directions, respectively [see Fig. 9(b)]. Therefore, the lowest-energy AFM1 configuration could be approximated as a one-dimensional (1D) AF alternating chain with weak AF interchain coupling, similar to the 1D $S = 1/2$ alternating AF chain system explored by the Bonner-Fisher-Heisenberg model [49]. Indeed, a broad maximum in the susceptibility data (near 280 K) has been observed above $T_N \sim 184$ K [see the inset of Fig. 2(b)], which suggests the existence of a short-range AF spin exchange for a low-dimensional system before reaching three-dimensional long-range ordering.

Although no Bonner-Fisher model for an $S = 5/2$ alternating chain is available in the literature, we tentatively ignore the difference between J_3 and J_4 and apply a homogeneous $S = 5/2$ Bonner-Fisher model to our system. The average intrachain coupling in the armchair-type AF chain can be extracted from the use of the following equation [50]:

$$\chi = \frac{Ng^2\mu_B^2}{k_B T} \frac{A + Bx^2}{1 + Cx + Dx^3}, \quad (2)$$

where $x = |J|/k_B T$, and J is negative for AF coupling. Here, N is Avogadro's number, k_B is Boltzmann's constant, g is the gyromagnetic ratio, and μ_B is the Bohr magneton. Using the analytical coefficients for an $S = 5/2$ spin system [50] to fit the high-temperature data shown in the inset of Fig. 2(b), we obtain $J/k_B = -27.2$ K, which is in fairly good agreement with the theoretically calculated value of $J_4/k_B = -23.93$ K.

4. Preferred oxygen vacancy site

In this section, we use first principles calculations to explore the issue of oxygen vacancies in CaFe_2O_4 , and their effects on the magnetic properties.

We first examine the possible oxygen vacancy sites and the corresponding energetics. If we consider the symmetries of the crystal structure and make the further assumption that the Fe(1) and Fe(2) sites are equivalent, there are four inequivalent oxygen sites. A single O vacancy was introduced at, in turn, a single one of each of these sites of a $\text{Ca}_{64}\text{Fe}_{128}\text{O}_{256}$ AFM1 supercell. This corresponds to a sufficiently large supercell to avoid introducing a spurious interaction between defects in the neighboring cells due to periodic boundary conditions. Moreover, the vacancy partial pressure and the need to relax the lattice constants can be neglected at such low vacancy concentrations.

The vacancy formation energy was computed using the equation $\Delta E = E_{\text{vac}} + E_{\text{O}} - E_{\text{bulk}}$, where E_{bulk} and E_{vac} are the total energies of the stoichiometric and nonstoichiometric supercells, respectively, and $E_{\text{O}} = E_{\text{O}_2}/2$. Here, E_{O_2} is the total energy of an isolated O_2 molecule in the gas phase; special care was taken to ensure that the O_2 molecule was in its triplet ground state when calculating this. In the vacancy structures, we have handled the different oxidation states of Fe by following the methodology proposed by Alavi *et al* [51].

Figure 8(a) shows the four inequivalent oxygen sites that we have considered for the analysis of vacancy formation. Notably, the creation of a single O vacancy breaks two different superexchange pathways simultaneously. The removal of an oxygen atom from an O1 site results in the elimination of one superexchange interaction of type J_1 , along with one interaction of type J_{b1} between two nearest-neighbor Fe ions in an $\text{Fe}(1)\text{O}_6$ octahedron. A vacancy at an O2 site removes a J_2 and a J_{b2} . Similarly, vacancies at O3 and O4 sites remove J_3 , J_{b1} and J_4 , J_{b2} interactions, respectively. By optimizing both the spin configuration and the atomic positions in these cases, all four vacancy structures are found to be FI with a net magnetic moment ranging from $12 \mu_B$ to $13.3 \mu_B$ per vacancy site (see Table III). The vacancy formation energy

TABLE III. Vacancy formation energy E_{vac} and net magnetic moment μ_{vac} for a single oxygen vacancy created at four inequivalent vacancy sites of a $2 \times 2 \times 2$ supercell, as labeled in Fig. 8(a).

vacancy site	E_{vac} (eV)	μ_{vac} (μ_B)
O1	4.30	12.0
O2	4.00	12.0
O3	4.23	12.0
O4	4.68	13.3

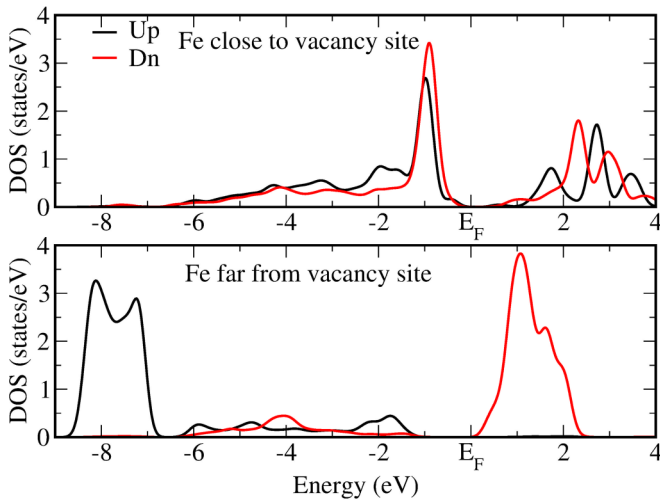


FIG. 10. Density of states (DOS) projected onto the Fe-3d orbital for (top) Fe close to O2 vacancy site and for (bottom) Fe far from O2 vacancy site [see Fig. 9(a)]. In (a), nearly equal DOS for up and down spins exists below the Fermi level, which indicates the LS state corresponding to Fe ions, whereas for (b), only the up-spin state is completely occupied deep below the Fermi level, indicating the HS state.

corresponding to the site O2 is found to be the lowest, $\Delta E = 4.00$ eV.

To quantify the charges associated with the different Fe ions in these vacancy configurations, we perform a Bader analysis, based on the electronic charge density [52,53]. For the case in which the vacancy is in the O2 position, we find that the electronic valence charge associated with the three Fe sites closest to the vacancy is 6.64 electrons per Fe site, whereas the charge associated with the Fe sites farther away from the vacancy site is 6.09 electrons. In an ideal ionic environment, one expects the charge associated with Fe^{2+} and Fe^{3+} states to be 6 and 5 electrons, respectively. Clearly, our result shows a higher estimation of charges than those expected within the assumption of perfectly ionic bonds. This could be because the Bader method does not work very well in some covalent compounds and/or because one indeed does not have the ideally expected +2 and +3 charge states in this compound. However, our analysis clearly suggests the presence of two different types of oxidation states of Fe, as expected by the requirement of charge neutrality.

To gain insight into the spin configurations of these two types of Fe ions, the electronic density of states (DOS), projected onto the Fe 3d orbitals, is plotted in Fig. 10. In this figure, the lower panel shows the results for Fe ions that lie far from the vacancy site: one finds that the majority spin channels (plotted black online) lie deep below the Fermi level and are completely occupied, whereas the minority spin channels (red online) are completely unoccupied. This orbital occupancy is consistent with the HS and nominal +3 oxidation state of Fe ions. In contrast, the projected DOS for Fe ions near the vacancy site shows a completely different profile.

Both the majority and minority spin channels contribute almost equally near the Fermi level, and the corresponding net magnetic moment associated with such Fe ions is found to be $\sim 0.3 \mu_B$. Taking together the results from our Bader analysis and the projected DOS, we can identify these Fe ions to be in the nominal +2 oxidation state with a low spin configuration.

Thus, our theoretical results validate the experimental conclusion that oxygen vacancies in $\text{CaFe}_2\text{O}_{4-\delta}$ generate a fraction of Fe^{2+} ions in the LS state, whereas the majority of the remaining Fe^{3+} ions are in the HS state, and the net magnetic moment arises from an incomplete cancellation when these two types of ions are arranged antiferromagnetically in the randomly distributed FI clusters. As observed in $\text{CaFe}_2\text{O}_{4-\delta}$, only $\sim 15 - 42\%$ of the Fe (2) sites are in Fe^{2+} (LS) state due to oxygen deficiency in the structure [Figs. 3(b) and 8(a)].

IV. CONCLUSIONS

Our combined dc and ac magnetic susceptibility measurements on single-crystal and powder samples of calcium ferrite suggest the presence of FI ordering below $T_N \sim 184$ K. Both experiments and first principles calculations suggest that this is due to the presence of inhomogeneous oxygen vacancies, with the resulting magnetic structure arising from an AF ordering between a large number of Fe^{3+} ions in an HS state and a small number of Fe^{2+} ions in a low-spin state; the incomplete cancellation between these results in a net FI moment.

The superexchange coupling coefficients J_i have been obtained theoretically by fitting a Heisenberg model to the results of spin-polarized DFT calculations. The majority of the exchange coupling constants J_i thus obtained are negative (favoring AF alignment of spins), and their variation with Fe-O-Fe bond angle is in good agreement with the GK rules. The exchange couplings with the largest magnitude are J_3 and J_4 ; they connect adjacent Fe atoms that lie along the zigzag chains parallel to the b axis.

Although CaFe_2O_4 can be described crystallographically as a three-dimensional material composed of hexagonal tubes running parallel to the b axis and arranged in a honeycomb network, the effective magnetic structure, as determined by the most important (super)exchange interactions, is quite different. If one considers the J_i values, it becomes more natural to view the material as being composed of stacked two-dimensional planes, with each plane composed of antiferromagnetically coupled armchair-type chains extending along the a direction.

ACKNOWLEDGMENTS

F.C.C. acknowledges support from Ministry of Science and Technology, Taiwan (MOST) under proposal number 106-2119-M-002-035-MY3. R.D. acknowledges support from National Taiwan University post doctoral research fellowship under Project Number 104R4000.

- [1] B. F. Decker and J. S. Kasper, *Acta Cryst.* **10**, 332 (1957).
- [2] J. Cao, J. Xing, Y. Zhang, H. Tong, Y. Bi, T. Kako, M. Takeguchi, and J. Ye, *Langmuir* **29**, 3116 (2013).
- [3] H. R. Ong, Md. M. R. Khan, A. Yousuf, N. A. Hussaina, and C. K. Chenga, *RSC. Adv.* **5**, 100362 (2015).
- [4] D. Hirabayashi, T. Yoshikawa, Y. Kawamoto, K. Mochizuki, and K. Suzuki, *Adv. Sci. Technol.* **45**, 2169 (2006).
- [5] Y. Matsumoto, M. Omae, K. Sugiyama, and E. Sato, *J. Phys. Chem.* **91**, 577 (1987).
- [6] S. Ida, K. Yamada, T. Matsunaga, H. Hagiwara, Y. Matsumoto, and T. Ishihara, *J. Am. Chem. Soc.* **132**, 17343 (2010).
- [7] R. A. Candeia, M. I. B. Bernardib, E. Longoc, I. M. G. Santosa, and A. G. Souzaa, *Mat. Lett.* **58**, 569 (2004).
- [8] A. Lashtabega and S. J. Skinner, *J. Mater. Chem.* **16**, 3161 (2006).
- [9] Y. Miura, R. Hirai, Y. Kobayashi, and M. Sato, *J. Phys. Soc. Jpn.* **75**, 084707 (2006).
- [10] M. J. Geselbracht, A. S. Erickson, M. P. Rogge, J. E. Greedan, R. I. Walton, M. W. Stoltzfus, H. W. Eng, and P. M. Woodward, *J. Solid State Chem.* **179**, 3489 (2006).
- [11] O. Pieper, B. Lake, A. Daoud-Aladine, M. Reehuis, K. Prokeš, B. Klemke, K. Kiefer, J. Q. Yan, A. Niazi, D. C. Johnston, and A. Honecker, *Phys. Rev. B* **79**, 180409(R) (2009).
- [12] F. Damay, C. Martin, V. Hardy, A. Maignan, G. André, K. Knight, S. R. Giblin, and L. C. Chapon, *Phys. Rev. B* **81**, 214405 (2010).
- [13] B. D. White, J. A. Souza, C. Chiorescu, J. J. Neumeier, and J. L. Cohn, *Phys. Rev. B* **79**, 104427 (2009).
- [14] C. D. Ling, J. J. Neumeier, and D. N. Argyriou, *J. Solid State Chem.* **160**, 167 (2001).
- [15] M. Shizuya, M. Isobe, and E. T. Muromachi, *J. Solid State Chem.* **180**, 2550 (2007).
- [16] E. Greenberg, G. K. Rozenberg, W. Xu, M. P. Pasternak, C. McCammon, K. Glazyrin, and L. S. Dubrovinsky, *Phys. Rev. B* **88**, 214109 (2013).
- [17] L. M. Corliss, J. M. Hastings, and W. Kunmann, *Phys. Rev.* **160**, 408 (1967).
- [18] C. Stock, E. E. Rodriguez, N. Lee, M. A. Green, F. Demmel, R. A. Ewings, P. Fouquet, M. Laver, Ch. Niedermayer, Y. Su, K. Nemkovski, J. A. Rodriguez-Rivera, and S.-W. Cheong, *Phys. Rev. Lett.* **117**, 017201 (2016).
- [19] H. Watanabe, H. Yamauchi, M. Ohashi, M. Sugimoto, T. Okada, and M. Fukase, *J. Phys. Soc. Japan.* **22**, 939 (1967).
- [20] A. Maljuk, J. Stremper, and C. T. Lin, *J. Crystal Growth* **258**, 435 (2003).
- [21] R. Das, S. Karna, Y. C. Lai, and F.-C. Chou, *Cryst. Growth Des.* **16**, 499 (2016).
- [22] E. V. Tsipis, Y. V. Pivak, J. C. Waerenborgh, V. A. Kolotygin, A. P. Viskup, and V. V. Kharton, *Solid State Ionics* **178**, 1428 (2007).
- [23] L. S. Lobanovsky and S. V. Trukhanov, *Crystallography Reports* **56**, 482 (2011).
- [24] S. Zouari, L. Ranno, A. Cheikh-Rouhou, M. Pernet, and P. Strobel, *J. Mater. Chem.* **13**, 951 (2003).
- [25] P. W. Selwood, *Magnetochemistry*, 2nd ed. (Wiley-Interscience, New York, 1956), pp. 78.
- [26] G. A. Bain and J. F. Berry, *J. Chem. Edu.* **85**, 532 (2008).
- [27] R. M. White, *Quantum Theory of Magnetism* (Springer, New York, 2006).
- [28] R. Sankar, G. J. Shu, B. Karunakara Moorthy, R. Jayavel, and F. C. Chou, *Dalton Trans.* **42**, 10439 (2013).
- [29] T. Moriya, *Phys. Rev.* **117**, 635 (1960).
- [30] A. H. Cooke, K. A. Gehring, and R. Lazenby, *Proc. Phys. Soc.* **85**, 967 (1965).
- [31] R. P. Feynman, R. B. Leighton, and M. L. Sands, *The Feynman Lectures on Physics*, Vol. I. (California Inst. of Technology, Addison-Wesley, USA, 1963).
- [32] C. A. M. Mulder, A. J. van Duynveldt, H. W. M. van der Linden, B. H. Verbeek, J. C. M. van Dongen, G. J. Nieuwenhuys, and J. A. Mydosh, *Phys. Lett. A* **83**, 74 (1981).
- [33] C. A. M. Mulder, A. J. van Duynveldt, and J. A. Mydosh, *Phys. Rev. B* **23**, 1384 (1981).
- [34] H. Yamamoto, T. Okada, H. Watanabe, and M. J. Fukase, *J. Phys. Soc. Jpn.* **24**, 275 (1968).
- [35] T. Y. Ou-Yang, G. J. Shu, C. D. Hu, and F. C. Chou, *J. Appl. Phys.* **117**, 123903 (2015).
- [36] G. Kresse and J. Hafner, *Phys. Rev. B* **47**, 558 (1993); G. Kresse and J. Furthmüller, *ibid.* **54**, 11169 (1996).
- [37] G. Kresse and J. Furthmüller, *Comput. Mater. Sci.* **6**, 15 (1996).
- [38] P. E. Blochl, *Phys. Rev. B* **50**, 17953 (1994).
- [39] G. Kresse and D. Joubert, *Phys. Rev. B* **59**, 1758 (1999).
- [40] J. P. Perdew, K. Burke, and M. Ernzerhof, *Phys. Rev. Lett.* **77**, 3865 (1996).
- [41] J. P. Perdew, K. Burke, and M. Ernzerhof, *Phys. Rev. Lett.* **78**, 1396 (1997).
- [42] S. L. Dudarev, G. A. Botton, S. Y. Savrasov, C. J. Humphreys, and A. P. Sutton, *Phys. Rev. B* **57**, 1505 (1998).
- [43] K. Obata, Y. Obukuro, S. Matsumita, H. Nakamura, M. Arai, and K. Kobayashi, *J. Ceram. Soc. Jap.* **121**, 766 (2013).
- [44] J. B. Goodenough, *J. Phys. Chem. Sol.* **6**, 287 (1958).
- [45] J. Kanamori, *J. Phys. Chem. Sol.* **10**, 87 (1959).
- [46] P. W. Anderson, *Phys. Rev.* **115**, 2 (1959).
- [47] J. S. Smart, *Effective Field Theory of Magnetism* (W. B. Saunders, Philadelphia, 1966).
- [48] See Supplemental Material at <http://link.aps.org/supplemental/10.1103/PhysRevB.98.144404> for the derivation of Weiss temperature for Antiferromagnetic systems.
- [49] J. C. Bonner, H. W. J. Blote, J. W. Bray, and I. S. Jacobs, *J. Appl. Phys.* **50**, 1810 (1979).
- [50] W. Hiller, J. Strahle, A. Datz, M. Hanack, W. E. Hatfield, L. W. ter Haar, and P. Gütllich, *J. Am. Chem. Soc.* **106**, 329 (1984).
- [51] C. Zhang and A. Alavi, *J. Am. Chem. Soc.* **127**, 9808 (2005).
- [52] R. F. W. Bader, *Atoms in Molecules: A Quantum Theory* (International Series of Monographs on Chemistry Clarendon Press, Oxford, 1990).
- [53] G. Henkelman, A. Arnaldsson, and H. Jonsson, *Comput. Mater. Sci.* **36**, 354 (2006).